Materials Today Chemistry 14 (2019) 100185

Contents lists available at ScienceDirect

Materials Today Chemistry

journal homepage: www.journals.elsevier.com/materials-today-chemistry/

Polybenzimidazole nanofibers for neural stem cell culture

F.F.F. Garrudo [a, b, c], R.N. Udangawa [a], P.R. Hoffman [a], L. Sordini [b, c, d], C.A. Chapman [a], P.E. Mikael [a], F.A. Ferreira [b, c], J.C. Silva [a, b, c], C.A.V. Rodrigues [b, c], J.M.S. Cabral [b, c], J.M.F. Morgado [d], F.C. Ferreira [b, c], R.J. Linhardt [a, *]

[a] Center for Biotechnology and Interdisciplinary Studies, Department of Chemistry and Chemical Biology, Rensselaer Polytechnic Institute, Troy, NY, 12180-3590, United States
[b] Department of Bioengineering and iBB – Institute for Bioengineering and Biosciences, Instituto Superior Técnico, Universidade de Lisboa, Av. Rovisco Pais, P-1049-001, Lisboa, Portugal
[c] The Discoveries Centre for Regenerative and Precision Medicine, Lisbon Campus, Instituto Superior Técnico, Universidade de Lisboa, Av. Rovisco Pais, P-1049-001 Lisboa, Portugal
[d] Department of Bioengineering and Instituto de Telecomunicações, Instituto Superior Técnico, Universidade de Lisboa, P-1049-001, Lisboa, Portugal

ARTICLE INFO

Article history:
Received 9 June 2019
Received in revised form
29 July 2019
Accepted 22 August 2019
Available online xxx

Keywords:
Scaffolds
Electrospinning
Conductive polymers
Biocompatibility
Neural engineering
Regenerative medicine

ABSTRACT

Neurodegenerative diseases compromise the quality of life of an increasing number of people in the world's aging population. While diagnosis is possible, no effective treatments are available. Strong efforts are needed to develop new therapeutic approaches, namely, in the areas of tissue engineering and deep brain stimulation. Conductive polymers are the ideal material for these applications owing to the positive effect of conducting electricity on the neural cell's differentiation profile. This novel study assessed the biocompatibility of polybenzimidazole (PBI) as electrospun fibers and after being doped with different acids. First, doped films of PBI were used to characterize the materials' contact angle and electroconductivity. After this, fibers were electrospun and characterized by scanning electron microscopy, Fourier-transform infrared spectroscopy, and thermogravimetric analysis. Neural stem cell (NSC) proliferation was assessed, and their growth rate and morphology on different samples were determined. Differentiation of NSCs on PBI-β-camphorsulfonic acid (CSA) fibers was also investigated, and gene expression (SOX2, NES, GFAP, and Tuj1) was assessed through immunochemistry and quantitative real-time polymerase chain reaction. All the samples tested were able to support NSC proliferation without significant changes on the cell's typical morphology. Successful differentiation of NSCs toward neural cells on PBI-CSA fibers was also achieved. This promising PBI fibrous scaffold material is envisioned to be used in neural cell engineering applications, including scaffolds and *in vitro* models for drug screening and electrodes.

© 2019 Elsevier Ltd. All rights reserved.

1. Introduction

Neurological disorders affect the quality of life and autonomy of patients, their families, and society in general. They involve the irreversible loss of neural tissue, which in turn causes cognitive loss, movement impairment, and dementia. With the increase of the aging population, the social and economic burden of these diseases will rise. Current available therapies can only alleviate the symptoms; they cannot rescue or regenerate neural cells or cellular function [1].

The central nervous system has a high electrical activity. The use of electricity to direct the *in vitro* development of axons and neurites of neural cells has been widely studied [2,3]. *In vivo*, this can be achieved through deep brain stimulation (DBS), in which the brain tissue is electrically stimulated using temporary and directly implanted probes [4]. This technique allows not only the recording of brain activity but also the direct application of electricity to the brain tissue. The effects of DBS on neurological diseases, especially neurodegenerative ones such as Alzheimer and Parkinson disease, are promising, and complete clinical studies are required to assess their full clinical value [4–7]. Some challenges persist, including the fact that clinical assay must be performed directly on humans [5]. This means that materials used for these probes must be

* Corresponding author.
E-mail address: linhar@rpi.edu (R.J. Linhardt).

https://doi.org/10.1016/j.mtchem.2019.08.004
2468-5194/© 2019 Elsevier Ltd. All rights reserved.

biocompatible, allowing total integration of them in the brain tissue without damaging it, and must be electroconductive.

The combination of electrical stimulation and cell-supportive biomaterials is useful in enhancing the phenotype and functionality of *in vitro* cultured cells [3,8–10]. This strategy is largely used in tissue engineering, which can also be applied to the development of disease model platforms or transplants for direct integration in brain tissue [11]. The physicochemical and mechanical properties of these biomaterials have to be similar to those of the native tissue, boosting biocompatibility through successful tissue integration, for these biomaterials to be used in neural tissue therapies [12,13]. In fact, studies report that transplanted stiffer materials (e.g., metals) cause more tissue damage than softer materials such as polymers, hindering their performance in the long run [12,14,15].

Polymers can be shaped to better mimic the natural extracellular matrix (ECM) environment of the target tissue [3,13]. This includes diverse forms such as films [2], hydrogels [16,17], and fibers [18,19]. In particular, electroconductive polymers are a very interesting option because they are available to conduct electricity directly to adhered cells, benefiting their growth and differentiation [3,20,21]. However, conductive polymers are more versatile, cost less, and can be easily tailored/functionalized [22–24]. Some examples of conductive polymers include polypyrrole (PPy) [25], polyaniline (PANI) [26], and polyethylenedioxythiophene (PEDOT) [2].

In the last years, electrospun fibers gained a lot of attention mainly owing to nanofibers being able to structurally mimic the fibrillar structures present in the natural ECM [27,28]. Fibers made of conductive polymers, such as PPy and PANI, have been produced and not only were successfully demonstrated to be biocompatible but also increased the differentiation of neural stem cells (NSCs) when electricity was applied [29–31]. However, these polymers can only be electrospun using non-conductive carrier polymers (e.g., polycaprolactone (PCL)). This decreases the electroconductivity of the resulting fibers when compared with cast films of the neat materials. Furthermore, the process compromises the direct injection of electrical current and minimizes the positive effects of electrical stimulation of the cells [32,33].

Polybenzimidazole (PBI) is a fully aromatic heterocyclic conductive polymer. Many authors have described PBI as a chemically stable polymer and have shown that these imidazole derivatives are resistant to acid/basic treatment [34,35]. PBI can be degraded under thermooxidative conditions but not under acid or basic hydrolysis [36,37]. In fact, PBI can be doped using basic and acidic solutions to increase electroconductivity without observed degradation. The conditions under which PBI is stable include 0.1 M sodium hydroxide and 0.25 M hydrochloric acid (HCl) [38], up to 10 M sulfuric acid (H_2SO_4) and 10 M phosphoric acid for 24 h [39] and even 6 M potassium hydroxide [40].

One main advantage of PBI is that it can also be electrospun into nanofibers, but without the need for a carrier polymer [41,42]. However, to the best of our knowledge, biocompatibility data for this material cannot be found in the literature.

The aim of this work was therefore to evaluate the biocompatibility of electrospun PBI fibers for the first time. Different doping agents were used to modify the polymer's properties, including hydrophilicity and electroconductivity. After this, the obtained fibers were characterized. NSCs were used to assess this material's biocompatibility, through proliferation and differentiation assays. The study of this material's properties aims to increase the number of available biocompatible conductive materials. Its applications are numerous, including not only the design of new electric probes for DBS but also electroconductive scaffolds for drug screening and neural tissue engineering applications.

2. Materials and methods

2.1. Materials

The primary antibody anti-SOX2 was obtained from Abcam. Medical glue (Silastic® Medical Adhesive Silicone Type A) was obtained from Biesterfeld Spezialchemie Ibérica, SL. Ultralow attachment 24-well plates (flat bottom) were obtained from Corning. HCl (37%), isopropanol, H_2SO_4 (10 M), and sodium chloride (NaCl) were purchased from Fisher Scientific. Celazole® S26 polybenzimidazole in *N,N*-dimethylacetamide (DMAc) solution, containing 26 wt% PBI solids and 1.5 wt% lithium chloride, was purchased from PBI Performance Products. Paraformaldehyde (PFA [4% in phosphate-buffered saline {PBS}]; ChemCruz) was obtained from Santa Cruz Biotechnology. Anhydrous DMAc, β-camphorsulfonic acid (CSA), 4-(2-hydroxyethyl)-1-piperazineethanesulfonic acid (HEPES), 3-(4,5-dimethylthiazol-2-yl)-2,5-diphenyltetrazolium bromide (MTT), poly(L-ornithine hydrobromide) (MW: 30,000–70,000), glucose, human recombinant insulin, 2-(4-amidinophenyl)-6-indolecarbamidine dihydrochloride (DAPI), and osmium tetroxide (4% in H_2O) were purchased from Sigma. Dulbecco's phosphate-buffered saline (DPBS), Dulbecco's Modified Eagle's Medium (DMEM-F12 + glutamax [1X]); N2 supplement (100X); fetal bovine serum (FBS); pen-strep mixture (penicillin: 10,000 units/mL, streptomycin: 10,000 μg/mL); recombinant human epidermal growth factor (EGF); recombinant human fibroblast growth factor-2 (FGF-2); B27 supplement (50X); resazurin (Alamar Blue® cell viability reagent); calcein AM, LIVE/DEAD™ Fixable Red Dead Cell Stain Kit; normal goat serum (10%); triton X-100 (Surfact-Amps®, 10% in water); primary antibodies anti-Tuj1 (mouse), anti-GFAP (rat), and anti-Nestin (mouse); secondary antibodies Alexa 488 anti-mouse, Alexa 546 anti-rat, and Alexa 546 anti-rabbit; High-Capacity cDNA Reverse Transcription Kit; MicroAmp Fast Optical 96-well reaction plates; and TaqMan® assays for Tuj1 (Hs00801390_s1), GFAP (Hs00909233_m1), Nestin (Hs04187831_g1), SOX2 (Hs01053049_s1), and GAPDH (Hs02786624_g1) were obtained from Thermofisher. The RNA extraction kit was purchased from Zymo Scientific. A frozen stock of ReN-VM cells (Millipore) was used in these studies.

2.2. PBI solution preparation and film casting

PBI S26 solution was diluted to 13% using DMAc, and the mixture was left overnight under mechanical stirring to obtain a homogeneous solution. This solution was then casted onto a glassPs Petri dish and left in a vacuum oven for 4 h at 120 °C to effectively remove the solvent. Finally, the films were cooled overnight under atmospheric conditions before further processing.

2.3. Sample doping

PBI was doped by immersing the samples in aqueous solutions of H_2SO_4 (5 M), CSA (1 M), or HEPES (1.5 M) for 24 h. PBI soaked in a 0.41 M NaCl aqueous solution (0.41 M) was used as the control. Finally, the samples were washed three times with distilled water and dried overnight before further processing.

2.4. Film characterization

2.4.1. Electroconductivity

Four 50-nm-thick gold stripes were deposited using a thermal evaporation system (Edwards Coating System E 306A) to improve the electrical contact between doped PBI film samples and the measuring equipment. The electroconductivity of three different films was measured by the four-point probe method using a current

source (Keithley DC power source) and a multimeter (Agilent 34401A Multimeter). Finally, the thickness of the films was measured using a Dektak 3.21 profilometer.

2.4.2. Contact angle

Contact angle assessments were performed using a Kruss DSA25B goniometer, using the sessile drop technique and distilled water as the solvent. The spreading of the water droplet on different PBI film surfaces was assessed by measuring the contact angle of the droplet with the surface (n = 3). Drop Shape Analysis 4 software was used to take measurements every 5 s for 2 min.

2.5. Electrospinning

A 10-mL Luer lock syringe containing 13% PBI solution was connected using polytetrafluorethylene (PTFE) tubing to a 21G needle. The electrospinning process was performed under the following conditions: 30 kV direct current (DC) voltage, 0.5 mL h^{-1} flow rate, 16 cm from the tip of the needle to the static aluminum collector, temperature of 21 °C, and relative humidity of 50–55%. The samples were then left overnight to dry under atmospheric conditions and then doped as described in Section 2.3 before further processing.

2.6. Scanning electron microscopy

The morphology of the electrospun fiber mats was evaluated by scanning electron microscopy (SEM; Carl Zeiss Supra 55 FESEM) at 1 kV, after coating with a thin layer of platinum. The average diameter of the electrospun fiber samples was determined from SEM pictures of 100 individual fibers (25,000X, 20 fibers per image) using NIH ImageJ software (National Institutes of Health, MD, USA).

2.7. Attenuated total reflectance-Fourier-transform infrared spectroscopy

Attenuated total reflectance-Fourier-transform infrared spectroscopy (ATR-FTIR) spectra with 4 cm^{-1} resolution were obtained using the PerkinElmer Spectrum One FTIR spectrophotometer at room temperature. Transmittance was recorded from 650 to 4,000 cm^{-1} wavenumbers with an accumulation of 32 scans.

2.8. Thermogravimetric analysis

Thermal decomposition of the fiber mats was studied by thermogravimetric analysis (TGA) in a nitrogen/oxygen atmosphere (80:20) using a computer-controlled TA instrument (TGA Q5; New Castle, DE, USA). The samples placed in an alumina crucible were heated up to 150 °C for drying (10 min) at a heating rate of 20 °C min^{-1} and cooled back to room temperature. The dry samples were then subjected to thermal decomposition starting from 25 °C to 1,000 °C at a heating rate of 1.5 °C min^{-1}. For TGA, profiles of mass loss as a function of temperature were obtained and evaluated using TA Universal Analysis 2000 software (version 4.5A; TA Instruments). The onset temperature of degradation and corresponding mass losses were calculated for each sample using the first and second derivatives.

2.9. ISO 10993 cytotoxicity assays

Cytotoxicity tests were performed for electrospun PBI fibers (not doped) following the recommendations of ISO 10993-5 and 10993-12 guidelines. In brief, the mouse fibroblast cell line L-929 was cultured in DMEM containing 10% FBS and 1%antiapen-strep at 37 °C and 5% CO_2 until confluence before passage to 24-well plates at 150,000 cells cm^{-2} (direct contact) or 80,000 cells cm^{-2} (indirect contact). PBI fibers and latex (positive control) were sterilized using UV before further processing or incubated in DMEM for 24 h (6 cm^2 mL^{-1}) for lixiviate extraction (indirect contact). For direct contact, PBI fibers and latex were then placed on top of the cell's monolayer for 24 h before image analysis on an optical microscope (Leica microsystems CMS GmbH). For indirect contact, L-929 cells were incubated with lixiviates for 24 h, and cell viability was quantified using MTT assay. In brief, after washing with PBS, the cells were incubated with MTT solution (1 mg mL^{-1}) and left for incubation for 2 h at 37 °C. The resulting formazan salt was then dissolved using 0.1 M HCl in isopropanol, and absorbance was quantified at 570 nm. Cell viability was calculated using the negative control as the reference.

2.10. ReN-VM cell culture conditions

ReN-VM cells were used as a cell model of NSCs. They were grown on polyornithine (20 μg mL^{-1})- and laminin (10 μg mL^{-1})-coated plates in supplemented N2 medium at 37 °C and 5% CO_2 as recommended [2]. N2 medium is composed of DMEM/F12 with N2 supplement (1:100), additional glucose (1.6 g mL^{-1}), insulin (20 μg mL^{-1}), and icillintomycinpen-strep (1:100). The N2 medium was then supplemented with EGF (20 ng mL^{-1}), FGF-2 (20 ng mL^{-1}), and B27 (20 μL mL^{-1}).

2.11. ReN-VM cell proliferation and differentiation assays and kinetic data calculation

First, the electrospun fiber mats, fixed to glass coverslips with medical glue, were UV sterilized for 1.5 h per scaffold side and treated with 1% pen-strep solution in PBS for 3 h at 37 °C. They were then coated with polyornithine and laminin before seeding with ReN-VM cells (P10) at 20,000 cells cm^{-2}. The medium was added 1 h after seeding (37 °C and 5% CO_2) to promote initial cell attachment. The medium was exchanged on day 1 and every two days thereafter for 10-day duration until the end of the proliferation assay. Cellular metabolic activity was assessed using Alamar Blue® at days 3, 5, 7, and 10 for the proliferation assay. The equivalent cell number was determined using a calibration curve. Growth rate and doubling time were calculated using equations (1) and (2), respectively, assuming (after data examination) the exponential phase from day 3 to day 10.

$$Growth\ rate = \frac{[\ln(cells\ day\ 10) - \ln(cells\ day\ 3)]}{7\ days} \quad (1)$$

$$Doubling\ time = \frac{\ln 2}{Growth\ Rate} \quad (2)$$

2.12. LIVE/DEAD staining and SEM imaging

At the end of the proliferation assay, the cells were washed once with DPBS and then incubated with a staining solution composed of calcein (4 μM), Fixable Red Dead Cell Stain Kit (1 μL mL^{-1}), and glucose (0.056 M) in DPBS for 20 min at 37 °C. The cells were then washed, kept in DPBS supplemented with glucose (0.056 M), and imaged using a confocal microscope (Zeiss LSM 510META Spectral Confocal). After being fixed with 4% PFA, the cells were treated with 1% osmium tetroxide for 30 min in a qualified fume hood, dried using a critical point dryer (Supercritical Automegasamdri 915B, purge at 3), coated with platinum, and imaged by SEM (Carl Zeiss Supra 55 FESEM).

2.13. ReN-VM cell differentiation assay

The cells (56,000 cells cm^{-2}) were left to grow under the same conditions as the proliferation assay before switching N2 media for N2B27 media, inducing spontaneous differentiation of ReN-VM cells. The N2B27 medium is composed of a 1:1 mixture of N2 medium (no growth factors added) and B27 medium. The B27 medium is composed of neurobasal medium, B27 supplement (2:100), Glutamax (1:100), and penicillin-streptomycin (1:200). The medium was exchanged every two days until the end of the assay. Cellular metabolic activity was assessed using Alamar Blue® on days 1, 2, 4, and 8 to evaluate the number of cells present on the fibers.

2.14. Immunochemistry

After the differentiation assay, the cell samples from days 4 (end of proliferation) and 8 (end of differentiation) were fixed in 4% PFA for 10 min. They were then washed with DPBS twice and permeabilized with a blocking solution (10% goat serum and 0.2% Triton X-100 in DPBS) for 15 min at room temperature (RT). After another washing with DPBS, the cells were incubated with anti-Tuj1 (1:400), anti-GFAP (1:250), anti-Nestin (1:250), and anti-SOX2 (1:100) diluted in the staining solution (5% goat serum and 0.1% Triton X-100 in DPBS) overnight at 4 °C. This was followed by incubation of the secondary antibodies Alexa 488 anti-mouse (1:250), Alexa 546 anti-rat (1:250), and Alexa 546 anti-rabbit (1:250) diluted in the staining solution for 1 h at RT. Finally, DAPI (1 mg mL^{-1}) diluted in the staining solution was added for 5 min at 37 °C. The cells were then washed, kept in DPBS, and imaged using a confocal microscope (Zeiss LSM 510META Spectral Confocal). The obtained image stacks were then merged using ImageJ.

2.15. Quantitative real-time polymerase chain reaction

Quantitative real-time polymerase chain reaction (qPCR) was performed using TaqMan® gene expression assays. Tuj1 (neurons), GFAP (astrocytes), Nestin (NSCs), and SOX2 (stem cells) were chosen as the main interest targets. Gene expression in each group of the differentiation assay (days 4 and 8) was determined using the comparative Ct method and by normalizing the expression of each target gene to the endogenous reference transcript GAPDH.

2.16. Statistical analysis

All data are presented as mean values ± standard deviations. Statistical analysis was performed using Microsoft Excel. Significant differences between groups were measured using the analysis of variance test, followed by post hoc analysis and Bonferroni correction. $p<0.05$ was considered statistically significant.

3. Results and discussion

3.1. Film contact angle and electroconductivity

PBI films were used to assess the effects of doping treatments on their electroconducting and surface properties. In this work, after initial screening, 3 different acids with different pKa values were chosen to test the modification of the polymer's electroconductivity: H_2SO_4, CSA, and HEPES. Doping PBI with strong acids enables the modification of the polymer's properties, whereas the use of a NaCl solution is expected not to. Considering tissue engineering applications, contact angle is essential to evaluate surface wettability [43]. Electroconductivity changes, important for neural cell therapy applications, were also investigated.

Changes in PBI's contact angle were observed (Table 1 and Fig. S1). Treatment with H_2SO_4 increased PBI's hydrophilicity as a reduction in the contact angle from 45° to 39° was observed. The opposite was observed when PBI was treated with the organic acids CSA and HEPES, leading to an increase in contact angle to 51° and 71°, respectively. Treatment of the films with NaCl (saline control) led to an increase in the contact angle (from 45° to 60°). Apart from HEPES-treated samples, the variations observed vs. untreated PBI films were not statistically significant.

Changes in electroconductivity were also observed. PBI films' electroconductivity averaged 9.0×10^{-8} S cm^{-1}. When treated with H_2SO_4, electroconductivity increased to 2.4×10^{-4} S cm^{-1}, almost 10,000 times more than pristine PBI. Similar changes were reported in the literature [39,44]. When treated with other weaker acids (CSA and HEPES) and NaCl, we were not able to determine the films' electroconductivity. These samples are less conductive than pristine PBI, and were labeled as 'low.' We believe the bulk size of the doping agents used does not favor charge transport across PBI's chains and hence compromises the materials' electroconductivity. However, the immobilization of small organic molecules as doping agents in PBI opens the possibility of immobilizing other biopolymers and bioactive agents within PBI. Examples of this include hyaluronic acid, dextran sulfate, and deoxyribonucleic acid, and these are useful for tissue engineering applications [45–47].

3.2. Average fiber diameters

We successfully prepared nanofibers from a 13% PBI DMAc solution by electrospinning, with fiber mats showing some beads. Previous reports in the literature refer to bead formation, which was even regarded as a hallmark in PBI nanofiber formation [41]. Environmental conditions also played a major role in fiber formation. High relative humidity values (higher than 50%) were necessary for fiber formation. Humidity contributed to PBI fiber formation, and this observation is consistent with results obtained by other groups [41,48,49]. However, no explanation has yet been proposed for this phenomenon. DMAc, the solvent used to solubilize PBI, has a boiling point of 165 °C and is miscible with water. Most likely, removal of DMAc from the on-producing fibers might have been accelerated by the high humidity, in a phenomenon that might resemble the phase inversion method used for the PBI membrane [50,51]. This eased the fiber formation process and explains why no fibers were obtained when humidity was lower than 50%.

Fibers obtained on PBI solution electrospinning have diameters within the nanoscale range (Table 1 and Fig. 1). After their production, the fibers were doped in the same way as the films: the obtained fibers were immersed in a concentrated acidic solution for 24 h, following the protocol by Glipa et al. [39]. Both high concentration and long exposure time promote extensive doping of the

Table 1
Electroconductivity and contact angle of PBI films (and diameter of the PBI electrospun fibers) (mean ± SD) (*=p-value<0.05).

Films	Films		Fibers
	Contact angle (θ)	Electroconductivity (S cm^{-1})	Diameter (nm)
PBI	44.9 ± 2.1	$(9.0 \pm 1.9) \times 10^{-8}$	131 ± 37
PBI-H_2SO_4	39.3 ± 9.7	$(2.4 \pm 2.2) \times 10^{-4}$	204 ± 65*
PBI-CSA	51.3 ± 4.7	(Low)	203 ± 67*
PBI-HEPES	70.6 ± 4.2*	(Low)	183 ± 44*
PBI-NaCl	59.9 ± 8.6	(Low)	139 ± 33

PBI, polybenzimidazole; CSA, β-camphorsulfonic acid; HEPES, 4-(2-hydroxyethyl)-1-piperazineethanesulfonic acid; SD, standard deviation.

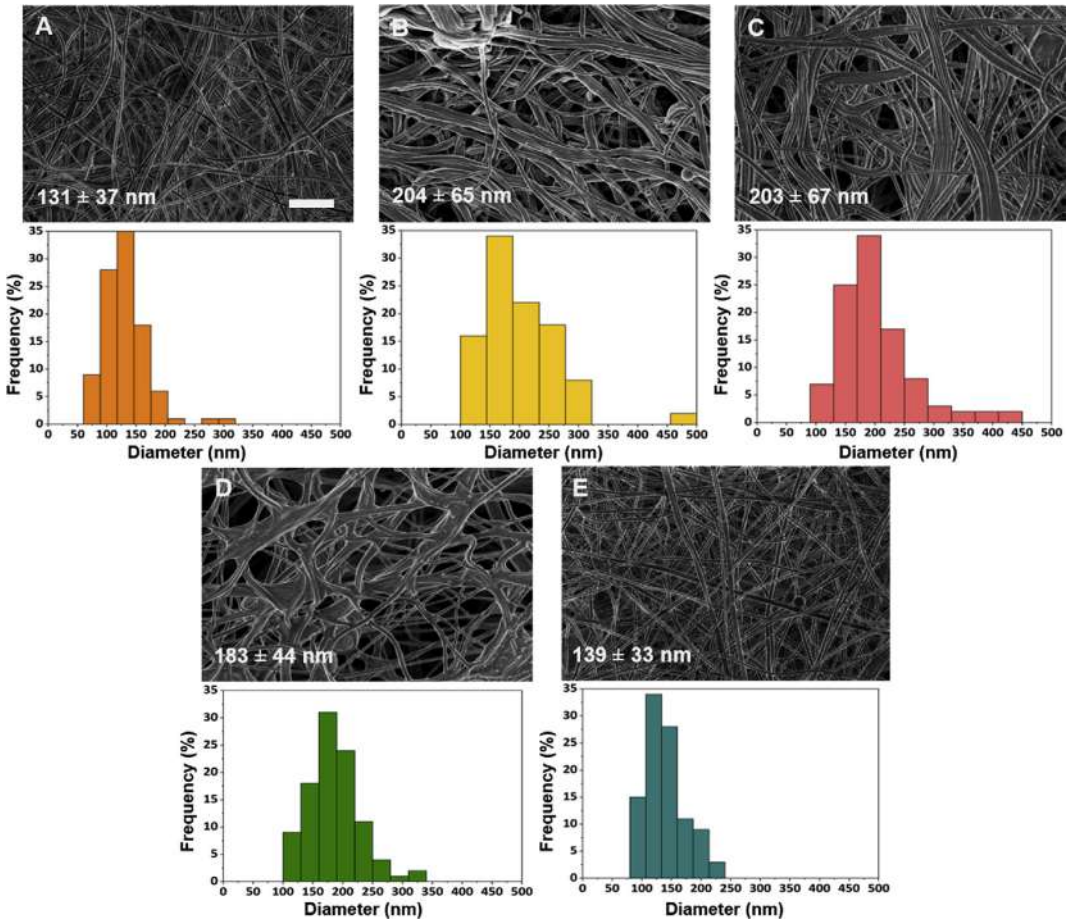

Fig. 1. SEM images and respective histograms (below) of PBI electrospun fibers. (A) Neat PBI fibers and fibers treated with (B) H_2SO_4, (C) CSA, (D) HEPES, and (E) NaCl (scale bar = 2 μm). PBI, polybenzimidazole; SEM, scanning electron microscopy; CSA, β-camphorsulfonic acid; HEPES, 4-(2-hydroxyethyl)-1-piperazineethanesulfonic acid.

polymer chain, enabling efficient physical properties change such as electroconductivity and contact angle [39,52].

The average diameter for untreated PBI fibers was 131 ± 37 nm and for those treated with NaCl was 139 ± 39 nm, which were not statistically different from each other. The increase in fiber average diameter was significant in the fibers treated with H_2SO_4 (204 ± 65 nm), CSA (203 ± 67 nm), and HEPES (183 ± 44 nm). The statistically significant changes observed in the fibers' diameters can have various possible explanations, including the direct incorporation of the bulky doping agents inside the fibers and between PBI chains, the electrostatic repulsion between charged amine groups and direct water retention. In fact, PBI is a hygroscopic material, and the change in the molecule's charge due to doping is also predicted to enable the samples' ability to retain more water, contributing to their diameter increase (swelling effect) [44]. Interestingly, only treatment of the fibers with acidic solutions leads to increase in PBI fibers' diameter, whereas NaCl treatment did not produce any statistically significant differences. This means that the presence of the doping agent inside PBI and changes in charge are the most plausible explanation for these changes. Finally, considering their small average diameter (inferior to 283 nm) is expected, according to the literature, the use of these fibers will enhance the proliferative potential of the cells [53].

3.3. Fiber's physical properties: ATR-FTIR and TGA

Successful doping of the PBI fibers was also confirmed by FTIR and TGA. FTIR spectra of PBI electrospun fibers, with and without doping, are depicted in Fig. 2. Spectra for pristine PBI and PBI treated with NaCl are very similar, confirming that doping is not possible with saline solutions. PBI spectra have intense aromatic peaks at 693 cm^{-1}, 799 cm^{-1}, and 1,000 cm^{-1} corresponding to a

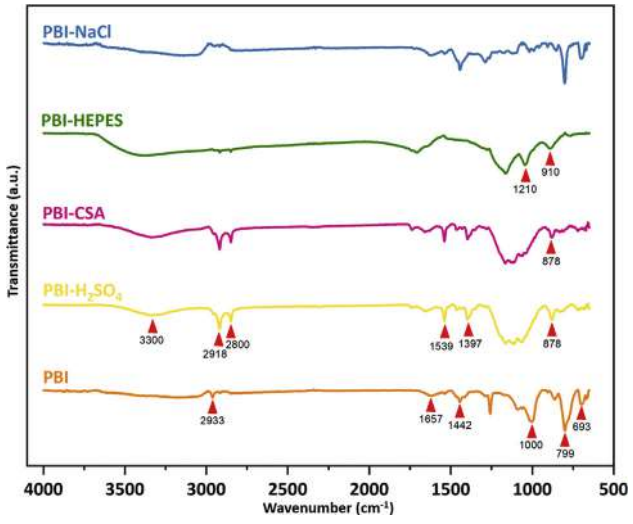

Fig. 2. ATR-FTIR profiles (resolution 4 cm^{-1}, 32 scans) for PBI fibers with no doping and doped with H_2SO_4, CSA, HEPES, and NaCl. ATR, attenuated total reflectance; FTIR, Fourier-transform infrared spectroscopy; PBI, polybenzimidazole; CSA, β-camphorsulfonic acid; HEPES, 4-(2-hydroxyethyl)-1-piperazineethanesulfonic acid.

substituted benzene ring, whereas PBI-NaCl only lacks the peak at 1,000 cm^{-1}. Peaks at 1,442 cm^{-1} and 1,657 cm^{-1} are also visible in PBI and PBI-NaCl spectra and correspond to in-plane deformation of the PBI ring and of the benzimidazole ring, respectively. Finally, a small peak at 2,933 cm^{-1}, which is attributed to a secondary amine salt group, and a wide region between 3,000 cm^{-1} and 3,650 cm^{-1} associated with amine groups widely distributed through the polymer's structure are visible in the spectra. Neither PBI nor PBI-NaCl shows ammonium ion and amine salt peaks at 1,397 cm^{-1} and 2,800/2,918 cm^{-1}, respectively. We correlate this to the absence of effective doping of the samples.

H_2SO_4 has a pKa of −3.9 and was previously described as a good doping agent for PBI [39]. Amine groups of PBI are protonated, forming ammonium groups that change the resonance structure of the polymer [39]. In this work, we hypothesize that other organic acids such as CSA (pKa = 1.2) and HEPES (pKa = 3.0), which are stronger acids than PBI (pKa = 5.23) could also serve as dopants [54].

For the samples treated with H_2SO_4 and CSA, aromatic peaks appeared at lower wavenumbers, namely, at 878 cm^{-1}, and in the wide area between 910 cm^{-1} and 1,210 cm^{-1}. The peak at 1,442 cm^{-1} for the PBI's ring deformation and the one at 1,657 cm^{-1} for the benzimidazole ring are still visible. Right next to them, new peaks can be identified at 1,397 cm^{-1} and 1,539 cm^{-1} corresponding to ammonium and secondary anime salt groups, respectively, both present in doped PBI. Finally, intense amine salt peaks at 2,800 cm^{-1} and 2,918 cm^{-1}, along with a narrower amine peak at 3,300 cm^{-1}, are visible. The HEPES spectrum mixes features of both doped and undoped PBI samples, namely, 2 broad aromatic (between 910 cm^{-1} and 1,210 cm^{-1}) and amine peaks (3,300 cm^{-1} area). Full doping does not occur for PBI-HEPES, as indicated by the low-intensity peaks for amine salt at 2,800 cm^{-1} and 2,918 cm^{-1}, evidencing that HEPES could not protonate PBI and therefore could not stabilize its resonance structure.

TGA data (Fig. 3 and Table S1) are different for fibers of pristine PBI and the doped ones. In our analysis, to better study PBI's degradation profile, water was previously removed from the samples through a heating cycle. Therefore, no water loss was observed on the samples as reported before in the literature [41]. When compared with neat PBI, mass loss for samples PBI-CSA and PBI-HEPES starts earlier (first onset temperatures: 298.6 °C and 255.9 °C, respectively). This is possibly due to an oxidative degradation of the doping agents or even to a loss of volatile components due to polycondensation reactions and then followed by PBI's chain degradation. For PBI-H_2SO_4, mass loss coincided with PBI's (414.9 °C vs 418.4 °C, respectively). For pristine PBI, three onset temperatures (418.4 °C, 438.8 °C, and 469.2 °C) were observed, whereas for the remaining samples, their single onset temperature was close to 429.9 ± 17.2 °C. It is plausible then to assume that the doping agents, and/or their degradation products, are responsible for the differences observed in the degradation profiles.

Both FTIR and TGA results demonstrate that doping is successful for H_2SO_4- and CSA-treated samples, partly complete for HEPES-treated samples and not effective for NaCl-treated samples. This shows that doping of PBI with acids less strong than H_2SO_4 is possible but impairs electroconductivity.

3.4. Cytotoxicity assay and cell proliferation analysis

The present work aimed at assessing PBI as a new support material for NSC growth and differentiation, which can then be used in DBS probe design. To the best of our knowledge, PBI's biocompatibility assessment, especially for neural tissue applications, has not been reported yet. Owing to its chemical stability, non-degradability, and ability to modify its electroconductive properties by doping, this material can also potentially be used in diverse biomedical applications, including the development of platforms for drug testing and biocompatible electronic implantable devices. It was therefore of paramount importance to assess this material's biocompatibility profile. Initially, standard ISO 10993 guidelines were followed to assess the material's biocompatibility using the murine fibroblast L-929 cell line, and the results are summarized in Fig. S2. The direct contact test did not reveal major morphological changes on the cells after contact with PBI electrospun fibers. The cell viability value obtained in the indirect contact (93.4 ± 4.7%) test showed PBI electrospun fibers to have passed the biocompatibility test (cutoff: 70%).

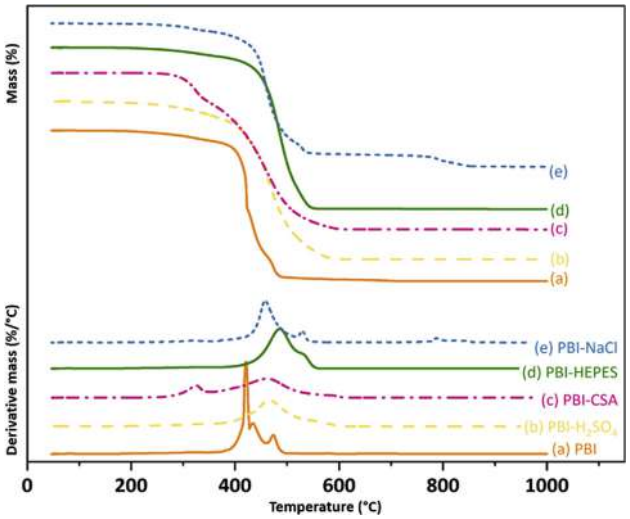

Fig. 3. TGA profiles (1.5 °C per min, 150–1,000 °C, with 20% oxygen) of PBI electrospun fibers, not doped or doped with H_2SO_4, CSA, HEPES, and NaCl, and respective first derivatives. TGA, thermogravimetric analysis; CSA, β-camphorsulfonic acid; HEPES, 4-(2-hydroxyethyl)-1-piperazineethanesulfonic acid; PBI, polybenzimidazole.

A proliferation assay with human-derived ReN-VM cells was the first approach used to assess PBI samples' biocompatibility. Fig. 4 displays the average equivalent number of cells calculated from fluorescence values obtained from Alamar Blue® at different timepoints of the proliferation assay. Overall, the obtained data show a constant increase in the number of cells for all the samples, including for the control glass coverslip samples. Proliferation data showed that ReN-VM cells were able to grow on all the samples throughout the timepoints tested. Cell numbers at day 10 show that PBI-CSA afforded a significantly higher number of cells at day 10. Taken these data into account, we calculated the respective kinetic data between days 3 and 10 for better comparison of the samples. The kinetic data are summarized in Table 2.

The kinetic values obtained were used to better compare the different samples at the end of the experiment. Despite the difference observed in cell numbers for glass and all PBI samples, overall growth rate values were higher on PBI fiber samples (undoped and doped), which led to shorter doubling times. We hypothesize that owing to its 3D structure and porous nature, PBI fibers can be remodeled by NSCs. This phenomenon, which appears to be independent of the doping agent used, might facilitate cell-cell contact and promote cell proliferation [55–57]. LIVE/DEAD images (Fig. 5(A)) of cells at day 10 show high viability of the cells by the end of the experiment. SEM images (Fig. 5(B)) show ReN-VM cells with their normal spindle/stellar shape adhered to the fiber mat, confirming that these cells were viable at the time they were fixed.

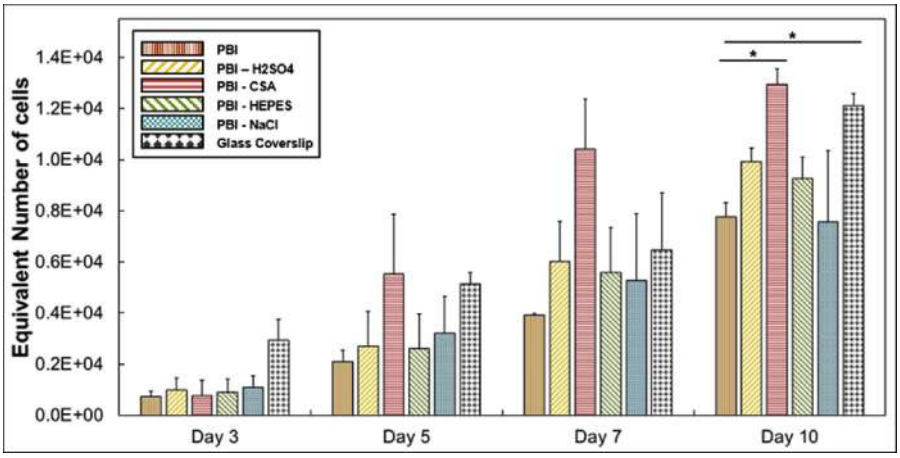

Fig. 4. Cell growth profile at days 3, 5, 7, and 10, using the equivalent number of cells (mean ± SD, n = 3) (* corresponds to $p<0.05$). Glass coverslips are used as controls. SD, standard deviation.

Table 2
Cell kinetic data, including growth rate and doubling time, for ReN-VM cells growing on different PBI fibers and glass coverslips.

Matrices	Growth rate (day^{-1})	Doubling time (h)
PBI	0.34 ± 0.06	49.5 ± 8.0
PBI-H_2SO_4	0.33 ± 0.08	50.4 ± 13.9
PBI-CSA	0.46 ± 0.18	41.4 ± 13.6
PBI-HEPES	0.35 ± 0.08	50.0 ± 13.3
PBI-NaCl	0.28 ± 0.01	59.5 ± 2.9
Glass coverslip	0.20 ± 0.05	83.2 ± 18.9

PBI, polybenzimidazole; CSA, β-camphorsulfonic acid; HEPES, 4-(2-hydroxyethyl)-1-piperazineethanesulfonic acid.

Previous research from Alba et al. [12] shows that cell interaction with PEDOT-coated DBS probes is important for tissue integration and better signal recording. Our material shows promising applications as a material for DBS or neural tissue engineering for the same reasons [12]. Overall, the previous data evidence that PBI is biocompatible toward ReN-VM cell expansion. Considering the favorable kinetic profile and the viability of the cultured cells, PBI-CSA samples were chosen for further studies.

3.5. Cell differentiation

To explore further biomedical applications of PBI, the ReN-VM cells were differentiated on PBI-CSA fibers. PBI-CSA was chosen for these studies owing to the higher growth rate value obtained. This allowed evaluation of the potential use of doped PBI in cell culture, which can be reproduced with other doping agents such as H_2SO_4 and phosphoric acid, depending on the envisaged application. The protocol included a 4-day proliferation period, followed by another 4-day period of differentiation. During this time, change from the supplemented N2 media used for proliferation to N2B27 media allowed the spontaneous differentiation of ReN-VM cells. The equivalent number of cells was also assessed throughout the process (Fig. S3).

Immunochemistry was used to evaluate neural gene expression (Fig. 6). At day 4, for both samples, no signal was detected for Tuj1, and GFAP had a low-intensity signal. High-intensity signals for both SOX2 and Nestin were also identified at day 4. There were visible changes at day 8, 4 days after differentiation was induced, namely, in cell morphology and marker expression. As for the cell's morphology, differentiated ReN-VM cells were able to spread through both substrates, without any specific orientation, were more elongated, and established a mesh of prolongments between the neighboring cells. While the cells were still expressing Nestin and SOX2 at similar or lower intensities, signals of both GFAP and Tuj1 substantially increased. Both GFAP and Tuj1 are commonly associated with astrocytes and neural cells but are interchangeably expressed in both cells at the immature stage [58–60]. However, differences in staining fluorescence intensity were evident for Tuj1 and GFAP and allowed to identify cells with these markers for

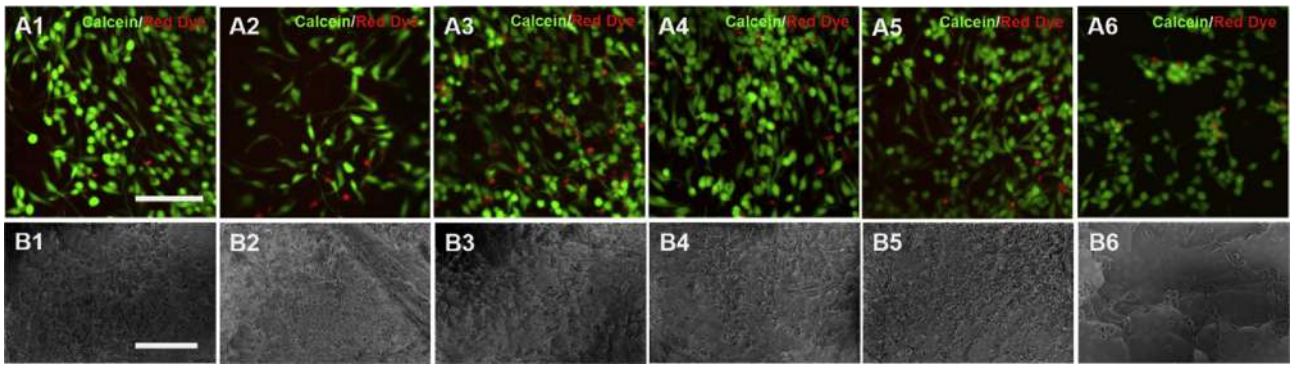

Fig. 5. LIVE/DEAD (A) and SEM (B) images of ReN-VM cells growing on PBI fibers, (1) with no doping or doped with (2) H_2SO_4, (3) CSA, (4) HEPES, or (5) NaCl. (6) Cells growing on glass coverslips were used as controls (scale bar = 100 μm). SEM, scanning electron microscopy; CSA, β-camphorsulfonic acid; HEPES, 4-(2-hydroxyethyl)-1-piperazineethanesulfonic acid; PBI, polybenzimidazole.

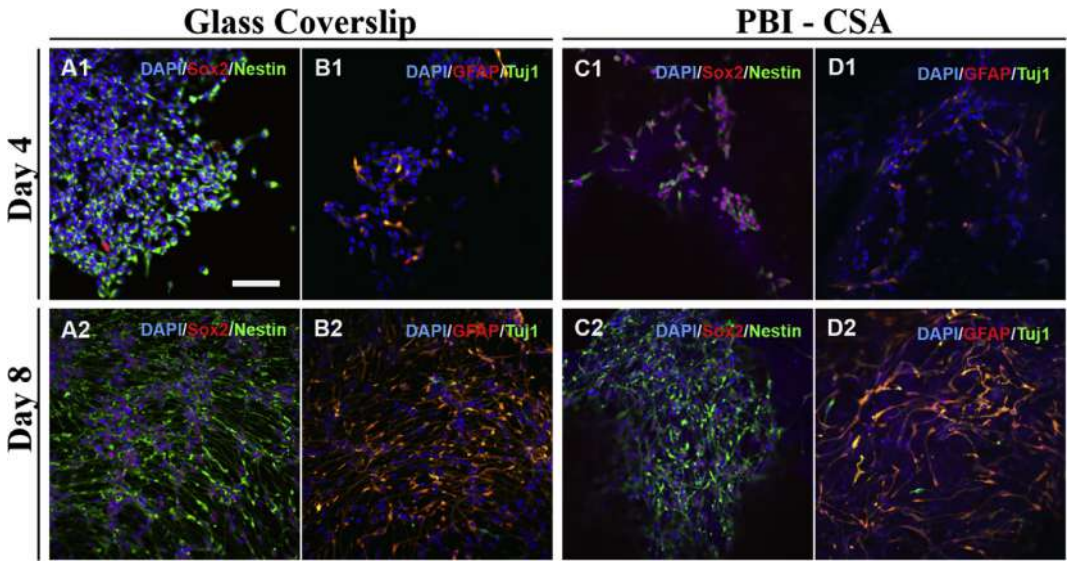

Fig. 6. Immunostaining of ReN-VM cells growing on glass (A and B) and PBI-CSA samples (C and D) at days 4 (1) and 8 (2) (scale bar = 100 μm). PBI, polybenzimidazole; CSA, β-camphorsulfonic acid.

differentiation toward neurons and astrocytes. SOX2 and Nestin are still present in the cells at day 8. Because these markers are specific for NSCs, their presence might be associated with an immature profile of the cells and/or cell-undifferentiated cell populations. These observations indicate that ReN-VM cells were differentiating into neuronal cells.

Samples from days 4 and 8 were also compared for their gene transcription activity by qPCR (Fig. 7). The genes analyzed were *sex-determining region Y-box 2* (SOX2) (ectoderm-derived stem cells), *Nestin* (NES) NSC(neural stem cells), *glial fibrillary acidic protein* (GFAP) (astrocytes), and *β-tubulin III* (Tuj1) (neurons). The results indicate that both cell groups growing on glass coverslips and PBI-CSA samples were able to differentiate toward neural cells. Gene transcription of SOX2, Nestin, GFAP, and Tuj1 increased for all the samples from day 4 to day 8. For SOX2, statistical differences were significant between days 4 and 8 for samples PBI-CSA and glass coverslip. Concerning Nestin, again differences were observed both for samples on PBI-CSA and glass coverslips between days 4 and 8, but those were only statistically significant for the latter. Concerning GFAP, increased expression in both PBI-CSA and glass coverslip samples from days 4 to 8 was statistically significant. Finally, for Tuj1, no statistically significant differences were observed between the samples, despite the visible increase in gene expression for both samples between the two timepoints.

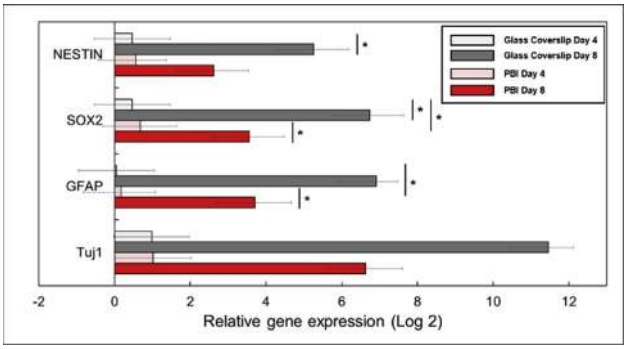

Fig. 7. qPCR analysis on gene expression of the neural genes Tuj1 and GFAP and the neural stem cell genes NES and SOX2 (n = 2) (mean ± SD) (*=*p*-value<0.05). qPCR, quantitative real-time polymerase chain reaction; SD, standard deviation; PBI, polybenzimidazole.

The results obtained from the qPCR experiments are in line with the immunostaining observation. Overall, gene expression of all the genes tested increased from day 4 to day 8, even in SOX2 and Nestin. This is correlated to an immature profile of the cells; an increase in these genes' expression is expected because of the short differentiation time. However, because GFAP and Tuj1 RNA levels increase during the same time frame, indicating early neural commitment, we could confirm that the differentiation process was taking place.

3.6. Final considerations

When considering biocompatibility alone, PBI fibers (with or without doping) performed better than glass coverslips regarding cell proliferation and differentiation. However, from an application point of view, differences between the two must be considered. PBI is a thermal and chemical-resistant polymer that can be easily processed into various flexible structures (fibers and films), and its physicochemical properties, such as contact angle and electroconductivity, can be fine-tuned by chemical doping. Although in this work we restricted the study only to three doping agents, other effective agents such as phosphoric acid can also be used.

The most abundant type of enzymes, present in the human extracellular environment, catalyzes the cleavage of ester (e.g., lipases), glycosidic (e.g., lysozyme), and peptide bonds (e.g., metalloproteases), and these are responsible for the ECM homeostasis. Because this polymer's structure does not resemble any major biological molecules or have any ester bonds in its structure, we do not expect PBI to biodegrade easily. Nevertheless, future studies should include a biodegradation profile assessment to determine this material's full potential in the field of biomedicine.

PBI shows promise in future biomedical applications based on all their studied features. Examples include the construction of electroconductive platforms for cultured cell stimulation suitable for cell expansion and the creation of *in vitro* models suitable for disease progression studies and drug screening. Owing to the biocompatibility profile of PBI and its ability to interact with living cells, its use in DBS probes also presents another promising

application. With regard to tissue engineering applications, PBI can also be viewed as a suitable candidate for the construction of electroconductive scaffolds/platforms for replacing electrically active organs (e.g., brain, heart) or even controlled drug delivery.

4. Conclusions

In summary, PBI fibers were successfully electrospun, doped with different acids, and characterized by FTIR and TGA. Doping PBI with strong acids increased the fibers' diameter, and its effects on electroconductivity and contact angle depended on the acid used. Both pristine and doped PBI fibers were able to support ReN-VM proliferation, and the cells managed to keep their normal spindle/stellar morphology. When induced, ReN-VM cells were also able to differentiate in neural cells on PBI-CSA fibers, showing a neuronal-like morphology and expressing neural cell markers. This work demonstrates that PBI is a biocompatible electroconductive polymer. These results open the way for the application of PBI in the design of neural cell–friendly platforms. These include not only DBS electrodes and other devices for the man-machine interface but also electroconductive scaffolds for tissue engineering applications and drug screening platforms.

Acknowledgments

The authors express gratitude to the Center for Biotechnology and Interdisciplinary Studies (CBIS), as well as the following CBIS core directors and the staff for their assistance in handling characterization instruments and data analysis: Analytical Core Facility (Joel Morgan, PhD), Microscopy Research (Sergey Pryshchep, PhD), and Nanoscale Characterization (Deniz Rende, PhD). The authors also thank the assistance from all the personnel from the MNCR-cMDIS-RPI cleanroom facility for SEM (Mr. David Frey, BSc) and 4-probe analysis (Bryant Colwill, BSc; Sarah An, PhD; John Barthel, BSc). F.F.F.G. and J.C.S. gratefully acknowledge the financial support from FCT (Fundação para a Ciência e Tecnologia) through the scholarships PD/BD/114045/2015 and SFRH/BD/105771/2014, respectively. F.A.F. acknowledges the financial support from CNPq-Brasil through the scholarship 205201/2014-8. The authors acknowledge the funding received by Institute for Bioengineering and Biosciences (iBB) from FCT (UID/BIO/04565/2013) and from Programa Operacional Regional (POR) Lisboa 2020 (Project N. 007317) and by IT from FCT (UID/EEA/50008/2019). The authors also thank the funding received from POR Lisboa 2020 through the project PRECISE – Accelerating progress toward the new era of precision medicine (Project N. 16394) and to Funacao para a Ciencia e Tecnología (FCT) Portugal through the project NEURON, PTDC/CTM-CTM/30237/2017. This work is also funded by the US National Institutes of Health, grant # DK111958 and New York State grant # SCRIB DOH01-PART2-2017.

Author contributions

F.F.F.G., R.N.U., P.H., L.S., C.A.C., and F.A.F. performed the study. F.C.F. proposed the original idea. F.F.F.G., P.E.M., J.M.F.M., F.C.F., and R.J.L. designed the experimental plan. F.F.F.G., J.C.S., and C.A.V.R. performed preliminary data experiments. J.M.S.C., J.M.F.M., F.C.F., and R.J.L. provided laboratory space. F.F.F.G., R.N.U., L.S., P.E.M., F.A.F., J.C.S., C.A.V.R., J.M.F.M., F.C.F., and R.J.L. contributed to the writing of the manuscript.

Conflicts of interest

No conflicts of interest to declare.

Appendix A. Supplementary data

Supplementary data to this article can be found online at https://doi.org/10.1016/j.mtchem.2019.08.004.

References

[1] J. Pettikiriarachchi, C. Parish, M. Shoichet, J. Forsythe, D. Nisbet, Biomaterials for brain tissue engineering, Aust. J. Chem. 63 (2010) 1143–1154.
[2] F. Pires, Q. Ferreira, C. Rodrigues, J. Morgado, F. Ferreira, Neural stem cell differentiation by electrical stimulation using a cross-linked PEDOT substrate: expanding the use of biocompatible conjugated conductive polymers for neural tissue engineering, Biochim. Biophys. Acta Gen. Subj. 1850 (2015) 1158–1168.
[3] K. Yang, S. Yu, J. Lee, H.-R. Lee, G.-E. Chang, J. Seo, et al., Electroconductive nanoscale topography for enhanced neuronal differentiation and electrophysiological maturation of human neural stem cells, Nanoscale 9 (2017) 18737–18752.
[4] W.-J. Neumann, R. Turner, B. Blankertz, T. Mitchell, A. Kühn, R. Richardson, Toward electrophysiology-based intelligent adaptive deep brain stimulation for movement disorders, Neurotherapeutics 16 (2019) 105–118.
[5] H. Roy, A. Green, T. Aziz, State of the art: novel applications for deep brain stimulation, Neuromodulation Technol. Neural Interface 21 (2018) 126–134.
[6] M. Bittlinger, S. Müller, Opening the debate on deep brain stimulation for Alzheimer disease–a critical evaluation of rationale, shortcomings, and ethical justification, BMC Med. Ethics 19 (2018) 1–23.
[7] A. Mann, E. Gondard, D. Tampellini, J. Milsted, D. Marillac, C. Hamani, et al., Chronic deep brain stimulation in an Alzheimer's disease mouse model enhances memory and reduces pathological hallmarks, Brain Stimul. 11 (2018) 435–444.
[8] A. Koppes, A. Seggio, D. Thompson, Neurite outgrowth is significantly increased by the simultaneous presentation of Schwann cells and moderate exogenous electric fields, J. Neural Eng. 8 (2011), 046023.
[9] W. Zhu, T. Ye, S.-J. Lee, H. Cui, S. Miao, X. Zhou, et al., Enhanced neural stem cell functions in conductive annealed carbon nanofibrous scaffolds with electrical stimulation, Nanomed. Nanotechnol. Biol. Med. 14 (2017) 2485–2494.
[10] P. Sensharma, G. Madhumathi, R.D. Jayant, A.K. Jaiswal, Biomaterials and cells for neural tissue engineering: current choices, Mater. Sci. Eng. C 77 (2017) 1302–1315.
[11] S. Kim, H. Lee, Y. Kim, Neural stem cell-based treatment for neurodegenerative diseases, Neuropathology 33 (2013) 491–504.
[12] N. Alba, Z. Du, K. Catt, T. Kozai, X. Cui, In vivo electrochemical analysis of a PEDOT/MWCNT neural electrode coating, Biosensors 5 (2015) 618–646.
[13] T.D.Y. Kozai, A.S. Jaquins-Gerstl, A.L. Vazquez, A.C. Michael, X.T. Cui, Brain tissue responses to neural implants impact signal sensitivity and intervention strategies, ACS Chem. Neurosci. 6 (2015) 48–67.
[14] D.-H. Kim, J. Wiler, D. Anderson, D. Kipke, D. Martin, Conducting polymers on hydrogel-coated neural electrode provide sensitive neural recordings in auditory cortex, Acta Biomater. 6 (2010) 57–62.
[15] M. Ganji, E. Kaestner, J. Hermiz, N. Rogers, A. Tanaka, D. Cleary, et al., Development and translation of PEDOT:PSS microelectrodes for intraoperative monitoring, Adv. Funct. Mater. (2017), 1700232.
[16] K. Zhang, Z. Shi, J. Zhou, Q. Xing, S. Ma, Q. Li, et al., Potential application of an injectable hydrogel scaffold loaded with mesenchymal stem cells for treating traumatic brain injury, J. Mater. Chem. B 6 (2018) 2982–2992.
[17] J. Shin, E. Choi, J. Cho, A.-N. Cho, Y. Jin, K. Yang, et al., Three-dimensional electroconductive hyaluronic acid hydrogels incorporated with carbon nanotubes and polypyrrole by catechol-mediated dispersion enhance neurogenesis of human neural stem cells, Biomacromolecules 18 (2017) 3060–3072.
[18] J.M. Zuidema, C. Provenza, T. Caliendo, S. Dutz, R. Gilbert, Magnetic NGF-releasing PLLA/iron oxide nanoparticles direct extending neurites and preferentially guide neurites along aligned electrospun microfibers, ACS Chem. Neurosci. 6 (2015) 1781–1788.
[19] F.F.F. Garrudo, C.A. Chapman, P.R. Hoffman, R.W. Udangawa, J.C. Silva, P.E. Mikael, et al., Polyaniline-polycaprolactone blended nanofibers for neural cell culture, Eur. Polym. J. 117 (2019) 28–37.
[20] R. Borah, G. Ingavle, S. Sandeman, A. Kumar, S. Mikhalovsky, Electrically conductive MEH-PPV:PCL electrospun nanofibres for electrical stimulation of rat PC12 pheochromocytoma cells, Biomater Sci. Uk 6 (2018) 2342–2359.
[21] O. Akhavan, Graphene scaffolds in progressive nanotechnology/stem cell-based tissue engineering of the nervous system, Artif. Organs 4 (2016) 3169–3190.
[22] W.M. Grill, S.E. Norman, R.V. Bellamkonda, Implanted neural interfaces: biochallenges and engineered solutions, Annu. Rev. Biomed. Eng. 11 (2009) 1–24.
[23] K.-A. Chang, J. Kim, J.A. Kim, S. Lee, S. Lee, S. Kim, et al., Biphasic electrical currents stimulation promotes both proliferation and differentiation of fetal neural stem cells, PLoS One 6 (2011), e18738.
[24] R. Balint, N. Cassidy, S. Cartmell, Conductive polymers: towards a smart biomaterial for tissue engineering, Acta Biomater. 10 (2014) 2341–2353.

[25] B. Thompson, R. Richardson, S. Moulton, A. Evans, S. O'Leary, G. Clark, et al., Conducting polymers, dual neurotrophins and pulsed electrical stimulation — dramatic effects on neurite outgrowth, J. Control. Release 141 (2010) 161–167.
[26] B. Xu, T. Bai, A. Sinclair, W. Wang, Q. Wu, F. Gao, et al., Directed neural stem cell differentiation on polyaniline-coated high strength hydrogels, Mater. Today Chem. 1 (2016) 15–22.
[27] A. Baji, Y.-W. Mai, S.-C. Wong, M. Abtahi, P. Chen, Electrospinning of polymer nanofibers: effects on oriented morphology, structures and tensile properties, Compos. Sci. Technol. 70 (2010) 703–718.
[28] W. Lu, J. Sun, X. Jiang, Recent advances in electrospinning technology and biomedical applications of electrospun fibers, J. Mater. Chem. B 2 (2014) 2369–2380.
[29] J. Wang, L. Tian, N. Chen, S. Ramakrishna, X. Mo, The cellular response of nerve cells on poly-l-lysine coated PLGA-MWCNTs aligned nanofibers under electrical stimulation, Mater. Sci. Eng. C 91 (2018) 715–726.
[30] L. Ghasemi-Mobarakeh, M.P. Prabhakaran, M. Morshed, M.H. Nasr-Esfahani, S. Ramakrishna, Electrical stimulation of nerve cells using conductive nanofibrous scaffolds for nerve tissue engineering, Tissue Eng. A 15 (2009) 3605–3619.
[31] Y. Li, X. Li, R. Zhao, C. Wang, F. Qiu, B. Sun, et al., Enhanced adhesion and proliferation of human umbilical vein endothelial cells on conductive PANI-PCL fiber scaffold by electrical stimulation, Mater. Sci. Eng. C 72 (2017) 106–112.
[32] S.I.A. Razak, I.F. Wahab, F. Fadil, F.N. Dahli, A.Z.M. Khudzari, H. Adeli, A review of electrospun conductive polyaniline based nanofiber composites and blends: processing features, applications, and future directions, Ann. Mater. Sci. Eng. (2015) 1–19.
[33] E.R. Holland, S.J. Pomfret, P.N. Adams, A.P. Monkman, Conductivity studies of polyaniline doped with CSA, J. Phys. Condens. Matter 8 (1996) 2991–3002.
[34] H. Vogel, C. Marvel, Polybenzimidazoles, new thermally stable polymers, J. Polym. Sci. 50 (1961) 511–539.
[35] R.B. Sandor, PBI (Polybenzimidazole): synthesis, properties and applications, High Perform. Polym. 2 (1990) 25–37.
[36] Musto, F.E. Karasz, W.J. MacKnight, Fourier transform infra-red spectroscopy on the thermo-oxidative degradation of polybenzimidazole and of a polybenzimidazole/polyetherimide blend, Polymer 34 (1993) 2934–2945.
[37] H.-Y. Li, Y.-L. Liu, Polyelectrolyte composite membranes of polybenzimidazole and crosslinked polybenzimidazole-polybenzoxazine electrospun nanofibers for proton exchange membrane fuel cells, J. Mater. Chem. 1 (2012) 1171–1178.
[38] F. Ferreira, T. Esteves, M. Carrasco, J. Bandarra, C. Afonso, F. Ferreira, Polybenzimidazole for active pharmaceutical ingredient purification: the Mometasone furoate case study, Ind. Eng. Chem. Res. 58 (2019) 10524–10532.
[39] X. Glipa, B. Bonnet, B. Mula, J. Deborah, J. Rozière, Investigation of the conduction properties of phosphoric and sulfuric acid doped polybenzimidazole, J. Mater. Chem. 9 (1999) 3045–3049.
[40] H. Hou, G. Sun, R. He, Z. Wu, B. Sun, Alkali doped polybenzimidazole membrane for high performance alkaline direct ethanol fuel cell, J. Power Sources 182 (2008) 95–99.
[41] Anandhan, Senthil Ponprapakaran, G. George, Parametric study of manufacturing ultrafine polybenzimidazole fibers by electrospinning, Int. J. Plast. Technol. 16 (2012) 101–116.
[42] C. Kim, Y.-J. Kim, Y.-A. Kim, Fabrication and structural characterization of electro-spun polybenzimidazol-derived carbon nanofiber by graphitization, Solid State Commun. 132 (2004) 567–571.
[43] Y. Arima, H. Iwata, Effect of wettability and surface functional groups on protein adsorption and cell adhesion using well-defined mixed self-assembled monolayers, Biomaterials 28 (2007) 3074–3082.
[44] Q. Li, R. He, R. Berg, H. Hjuler, N. Bjerrum, Water uptake and acid doping of polybenzimidazoles as electrolyte membranes for fuel cells, Solid State Ion. 168 (2004) 177–185.
[45] S. Wang, S. Guan, J. Wang, H. Liu, T. Liu, X. Ma, et al., Fabrication and characterization of conductive poly (3,4-ethylenedioxythiophene) doped with hyaluronic acid/poly (l-lactic acid) composite film for biomedical application, J. Biosci. Bioeng. 123 (2017) 116–125.
[46] D. Harman, R. Gorkin, L. Stevens, B. Thompson, K. Wagner, B. Weng, et al., Poly(3,4-ethylenedioxythiophene):dextran sulfate (PEDOT:DS) – a highly processable conductive organic biopolymer, Acta Biomater. 14 (2015) 33–42.
[47] A. Dawn, A. Nandi, Biomolecular hybrid of a conducting polymer with DNA: morphology, structure, and doping behavior, Macromol. Biosci. 5 (2005) 441–450.
[48] R. Walmsley, P. Hlangothi, C. Litwinski, T. Nyokong, N. Torto, Z. Tshentu, Catalytic oxidation of thioanisole using oxovanadium(IV)-functionalized electrospun polybenzimidazole nanofibers, J. Appl. Polym. Sci. 127 (2013) 4719–4725.
[49] T. Graberg, A. Thomas, A. Greiner, M. Antonietti, J. Weber, Electrospun silica—polybenzimidazole nanocomposite fibers, Macromol. Mater. Eng. 293 (2008) 815–819.
[50] J.S. Wainright, J.-T. Wang, D. Weng, R.F. Savinell, M. Litt, Acid-doped polybenzimidazoles: a new polymer electrolyte, J. Electrochem. Soc. 142 (1995).
[51] V. Kurdakova, E. Quartarone, P. Mustarelli, A. Magistris, E. Caponetti, M.L. Saladino, PBI-based composite membranes for polymer fuel cells, J. Power Sources 195 (2010) 7765–7769.
[52] I.B. Valtcheva, S.C. Kumbharkar, J.F. Kim, Y. Bhole, A.G. Livingston, Beyond polyimide: crosslinked polybenzimidazole membranes for organic solvent nanofiltration (OSN) in harsh environments, J. Membr. Sci. 457 (2014) 62–72.
[53] G. Christopherson, H. Song, H.-Q. Mao, The influence of fiber diameter of electrospun substrates on neural stem cell differentiation and proliferation, Biomaterials 30 (2009) 556–564.
[54] Q. Li, J.O. Jensen, R.F. Savinell, N.J. Bjerrum, High temperature proton exchange membranes based on polybenzimidazoles for fuel cells, Prog. Polym. Sci. 34 (2009) 449–477.
[55] P. Lu, K. Takai, V.M. Weaver, Z. Werb, Extracellular matrix degradation and remodeling in development and disease, Cold Spring Harb. Perspect. Biol. 3 (2011).
[56] C. Madl, B. LeSavage, C. Dinh, R. Dewi, R. Stowers, M. Khariton, et al., Maintenance of neural progenitor cell stemness in 3D hydrogels requires matrix remodelling, Nat. Mater. 16 (2017) 1233.
[57] C.M. Madl, S. c Heilshorn, Engineering hydrogel microenvironments to recapitulate the stem cell niche, Annu. Rev. Biomed. Eng. 20 (2018) 21–47.
[58] E. Dráberová, L. Valle, J. Gordon, V. Marková, B. Šmejkalová, L. Bertrand, et al., Class III β-tubulin is constitutively coexpressed with glial fibrillary acidic protein and Nestin in midgestational human fetal astrocytes: implications for phenotypic identity, J. Neuropathol. Exp. Neurol. 67 (2008) 341–354.
[59] K. Casper, K. McCarthy, GFAP-positive progenitor cells produce neurons and oligodendrocytes throughout the CNS, Mol. Cell. Neurosci. 31 (2006) 676–684.
[60] Namba Liu, Suzuki Liu, Seki Shioda, Glial fibrillary acidic protein-expressing neural progenitors give rise to immature neurons via early intermediate progenitors expressing both glial fibrillary acidic protein and neuronal markers in the adult hippocampus, Neuroscience 166 (2010) 241–251.